Stereochemical Insights into Sarpagan and Akuammiline Alkaloid Biosynthesis

Scott Galeung Alexander Mann, Malina Paz-Galeano, Mohammadamin Shahsavarani, Jacob Owen Perley, Jun Guo, Jorge Jonathan Oswaldo Garza-Garcia, and Yang Qu*

Department of Chemistry, University of New Brunswick, Fredericton, NB, E3B 5A3, Canada

*Correspondence: yang.qu@unb.ca

Abstract

The Apocynaceae family produces a remarkable diversity of monoterpenoid indole alkaloids (MIAs), many of which possess significant pharmaceutical value. Among these, sarpagan and akuammiline alkaloids represent distinct subclasses characterized by their intricate stereochemical frameworks, derived through enzymatically controlled cyclization and rearrangement of the key precursor geissoschizine. In this study, we systematically investigated the products and stereochemical outcomes of sarpagan bridge enzymes (SBEs) and rhazimal synthases (RHS), key enzymes involved in geissoschizine cyclization and MIA diversification. Using two previously characterized enzymes alongside five newly identified enzymes from six plant species, we demonstrate that RHS enzymes from *Alstonia scholaris*, *Vinca minor*, and *Amsonia tabernaemontana* exclusively produce the 16*R* rhazimal stereoisomer. In contrast, SBEs from *Catharanthus roseus*, *Vinca minor*, *Tabernaemontana elegans*, and *Rauvolfia serpentina* generate both 16*S* akuammidine aldehyde and 16*R* polyneuridine aldehyde diastereomers in varying ratios. Remarkably, downstream esterases and deformylases epimerize and alter the stereochemical configuration, yielding naturally occurring alkaloids bearing distinct C16 stereochemistry in different species. These findings are supported by both in vitro assays and *in planta* silencing of the newly identified *C. roseus* CrSBE, after we redirected the MIA flux to the otherwise muted sarpagan pathway. Our results provide a comprehensive understanding of the enzymatic control over C16 stereochemistry during SBE-mediated and RHS-mediated transformations. By elucidating how diastereomeric intermediates contribute to sarpagan MIA biosynthesis, this work addresses long-standing questions surrounding the stereochemical dynamics and enzymatic diversification of MIAs in nature.

Introduction

The Apocynaceae family is renowned for its exceptional diversity of monoterpenoid indole alkaloids (MIAs), a class of structurally complex and pharmaceutically significant natural products. Clinically important drugs, such as the anticancer drugs vinblastine and camptothecin, exemplify the therapeutic value of MIAs. [1] These compounds are categorized based on their carbon skeleton arrangements, which arise through distinct biosynthetic pathways. Among the diverse MIA subclasses, sarpagan and akuammiline alkaloids stand out due to their intricate stereochemical frameworks and pharmaceutical relevance. Notable examples include the antiarrhythmic drug ajmaline (sarpagan) and the natural analgesic akuammine (akuammiline). [2,3] Both alkaloid classes originate from the central precursor strictosidine (Fig. 1), undergoing enzymatically regulated cyclization, rearrangement, and modification steps to establish their defining chiral centers. Understanding these stereochemical pathways is vital, as the biological activities of these compounds often hinge on their precise three-dimensional configurations.

Upon deglycosylation, strictosidine generates a series of reactive, labile intermediates collectively known as strictosidine aglycone, which exist in equilibrium. Various cinnamyl alcohol dehydrogenase (CAD)-like reductases selectively reduce the iminium intermediates, leading to the formation of three major carbon skeletons: corynanthe, yohimbine, and heteroyohimbine with multiple stereochemical variations. [4–8] Among these, 19*E*-geissoschizine (Fig. 1) serves as a pivotal intermediate for the biosynthesis of three major MIA skeletons: strychnos, akuammiline, and sarpagan. [5,9] These skeletons differ in the site of C–C bond formation: C2–C16 for strychnos, C7–C16 for akuammiline, and C5–C16 for sarpagan, initiated by *N*4-oxidation and cyclization via the reactive 17-enol (Fig. 1). These reactions are catalyzed by homologous cytochrome P450 monooxygenases (CYPs), namely geissoschizine oxidase (GO) from *Catharanthus roseus*, rhazimal synthase (RHS) from *Alstonia scholaris*, and sarpagan bridge enzyme (SBE) from *Rauvolfia serpentina*, all of which have been cloned and functionally characterized in recent years. [2,6,10,11] Despite these advances, a significant gap remains regarding the stereochemical fate of C16 during the formation of these key bridges, particularly for the sarpagan and akuammiline skeletons.

The strychnos alkaloids, including akuammicine and norfluorocurarine, represent a smaller subset of MIAs where the original C16 stereochemistry from GO activity is eliminated during downstream transformations. For instance, spontaneous deformylation of GO product preakuammicine aldehyde iminium yields akuammicine (Fig. 1), while esterase-mediated decarboxylation generates norfluorocurarine, both intermediates for other MIA subclasses. [6,12] In contrast, tandem iminium and aldehyde reductions by CrRedox1 and CrRedox2 preserve the C16 stereochemistry in critical intermediates stemmadenine and *O*-acetylstemmadenine (Fig. 1). [6] However, reductase-mediated deacetylation induces C15–C16 bond cleavage, forming a C16–C17 alkene that again eliminates the original C16 stereochemistry. [6,13–17] The resulting dehydrosecodine serves as an intermediate to all iboga, aspidosperma, and pseudoaspidosperma alkaloids [2,6,13–15,18–20] , including the key monomers catharanthine and vindoline that undergo coupling to form the clinically important anticancer drug vinblastine in *C. roseus* (Fig. 1).

Geissoschizine's C7–C16 bridging can instead yield rhazinaline (16*S*) in *Rhazya stricta* [21] and rhazimal (16*R*), along with derivatives like akuammilline, picralinal, and strictamine in *C.*

roseus, *A. scholaris*, and *Vinca minor* (Fig. 1). [22–25] Similarly, the C5–C16 bridging, known as the sarpagan bridge, can theoretically generate both akuammidine aldehyde (16*S*) and polyneuridine aldehyde (16*R*). Downstream alkaloids may retain the akuammidine aldehyde stereochemistry, as seen in vobasine from *Tabernaemontana elegans*, [26] pericyclivine in *C. roseus*, [6] and sarpagine in *R. serpentina*, [27] while polyneuridine aldehyde stereochemistry is observed in alkaloids such as ajmaline and quebrachidine (Fig. 1). [2,28,29]

Our previous studies revealed that *C. roseus* GO produces exclusively 16*S* product, confirmed via 1D/2D Nuclear Magnetic Resolnance (NMR) studies, including Nuclear Overhauser Effect Spectroscopy (NOESY). [6] By contrast, *A. scholaris* AsRHS generates 16*R* stereochemistry, as evidenced by its alcohol derivative rhazimol, verified against synthetic standards. [11,30] However, the stereochemistry of SBE products remains experimentally uncharacterized, with conclusions thus far inferred only from downstream products.

In this study, we systematically investigated the products and stereochemical outcomes of SBE and RHS enzymatic reactions. By analyzing two previously characterized enzymes alongside five newly identified enzymes from six Apocynaceae species, we demonstrate that RHS enzymes from *A. scholaris*, *V. minor*, and *Amsonia tabernaemontana* exclusively produce the 16*R* rhazimal stereoisomer. In contrast, SBEs from *C. roseus*, *T. elegans*, *V. minor*, and *R. serpentina* generate both 16*S* akuammidine aldehyde and 16*R* polyneuridine aldehyde diastereomers in varying ratios. Notably, downstream esterases and deformylases epimerize C16 and shuffle the stereochemistry, leading to downstream alkaloids with distinct C16-configurations, such as ajmaline (polyneuridine stereochemistry) and pericyclivine/vobasine (akuammidine stereochemistry). Our findings are further supported by *in planta* silencing of a new enzyme *C. roseus* CrSBE, coupled with metabolically redirecting the biosynthetic flux to the otherwise muted sarpagan pathway in this plant. Our results provide a detailed and comprehensive understanding of SBE-mediated stereoisomer formation that has remained underexplored. By elucidating how diastereomeric precursors give rise to sarpagan MIAs in nature, this work addresses long-standing questions regarding the stereochemical dynamics driving MIA biosynthesis and diversification.

Results

CrSBE is necessary for 16*S*-sarpagan alkaloids biosynthesis in *C. roseus*

When we previously discovered and characterized CrGO, we examined the effects of silencing this enzyme in *C. roseus* leaves. CrGO silencing caused significant reduction of vindoline and catharanthine, downstream of the GO-product preakuammicine aldehyde iminium (Fig. 1). [6] We also observed a dramatic increase of pericyclivine and perivine, which typically accumulate at low levels. [6] These findings indicated a suppressed flux toward 16*S*-sarpagan MIAs due to strong CrGO activity.

The *C. roseus* leaf epidermis is the most important tissue for MIA formation and diversification. [31] After analyzing a *C. roseus* leaf epidermal transcriptome, [32] we identified an epidermis-specific GO homolog, which we designated as *C. roseus* Sarpagan Bridge Enzyme (CrSBE) based on subsequent experimental validation. The Expressed Sequence Tag (EST) counts, a

124 proxy for gene expression, were 38 and 8 for CrGO and CrSBE in epidermis, respectively. The
125 amino acid sequence of CrSBE was 51% identical to CrGO and 77% identical to *R. serpentina*
126 RsSBE2. [2] No additional GO or SBE homologs were detected in this transcriptome generated
127 from laser-dissected leaf epidermis. We hypothesized that CrSBE was responsible for 16*S*-
128 sarpagan alkaloid biosynthesis in *C. roseus* and conducted virus-induced gene silencing (VIGS)
129 experiments to investigate its function *in planta*. Given the low natural accumulation of 16*S*-
130 sarpagan alkaloids, co-silencing CrGO would elevate their levels to clearly demonstrate the
131 physiological relevance of CrSBE. Therefore, we silenced CrGO alone and used a single
132 chimeric VIGS construct for CrGO/SBE co-silencing.
133
134 Liquid Chromatography Tandem Mass Spectrometry (LC-MS/MS) and Quantitative Reverse
135 Transcription Polymerase Cyclization Reaction (qRT-PCR) experiments showed that silencing
136 CrGO transcripts by 89.6% resulted in 89.2% and 82.6% reduction of the two major alkaloids
137 catharanthine and vindoline/vindorosine (demethoxyvindoline) in *C. roseus*, respectively (Fig.1,
138 Fig. 2a-c), consistent with our previous findings. Similarly, vindolinine and epi-vindolinine, the
139 third most abundant MIAs, also decreased by 82.7%. In contrast, ajmalicine and serpentine
140 levels, which form prior to geissoschizine cyclization (Fig. 1), remained unchanged. In response
141 to significantly reduced GO levels, 19*E*-geissoschizine accumulated to 1.45 mg/g fresh leaf,
142 which was otherwise below detection limit in empty vector controls (Fig. 2b, c). In this
143 background, pericyclivine and perivine levels increased significantly, by 9.8-fold and 4.1-fold,
144 respectively, as free geissoschizine became available to CrSBE. Co-silencing GO and SBE by
145 64.5% and 95.9% (Fig. 2a), respectively, led to 97.5% and 92.2% reductions in pericyclivine and
146 perivine, alongside reductions in major MIAs and further accumulation of geissoschizine (Fig.
147 2a, b). These results indicated that CrSBE is physiologically responsible for the sarpagan
148 alkaloid biosynthesis in *C. roseus*.
149
150 Since polyneuridine aldehyde (16*R*) has been the only hypothetical product of SBE and
151 pericyclivine/perivine contain the opposite C16-stereochemistry, we carefully re-analysed the *C.*
152 *roseus* MIA chemistry. With LC-MS/MS, NOESY and other NMR experiments (Supplementary
153 fig. 1-7), we confirmed the C16-stereochemistry of pericyclivine purified from VIGS-GO plants.
154 [6] The up-field chemical shift of pericyclivine's carbomethoxy group (δ 3.02 ppm), caused by
155 indole shielding, is indicative for akuammidine 16*S* stereochemistry (Table 1 and 2). In NOESY
156 spectra, the H16, H5, and H15 cross peaks were also consistent with such stereochemistry. For
157 perivine, we confirmed its stereochemistry with a commercial standard, which could also be
158 enzymatically methylated to form vobasine (*N*4-methylperivine) with akuammidine 16*S*
159 stereochemistry as we previously determined by NOESY NMR. [26] These results revealed the
160 discrepancy between the hypothetical SBE product and the 16*S*-sarpagan alkaloid chemistry in
161 *C. roseus*, suggesting the production of the akuammidine aldehyde that would give rise to the
162 consistent stereochemistry in downstream products pericyclivine and perivine (Fig. 1).
163
164 **Sarpagan bridge enzymes from four species produce diastereomeric aldehydes at varying**
165 **ratios**
166
167 *C. roseus* exclusively accumulates 16*S* sarpagan MIAs without any known 16*R* sarpagan MIAs
168 or derivatives. Similarly, in *T. elegans*, the primary MIA is the 16*S*-sarpagan vobasine, with no
169 evidence of 16*R* sarpagan MIAs. [26,33] In comparison, *Rauvolfia* and *Vinca* species produce both

16*S* derivatives, such as akuammidine and sarpagine, and 16*R* derivatives, such as quebrachidine, vincamajine (*N*1-methylquebrachidine), 11-hydroxypolyneuridinne, and ajmaline. [27,34–37] This stereochemical variation further prompted us to investigate the stereochemistry of SBE products.

We expressed CrSBE, two new *T. elegans* and *V. minor* orthologs TeSBE and VmSBE, and a previously studied *R. serpentina* RsSBE2, sharing 72-82% amino acids identity among each other, in yeast to evaluate their in vitro activities. A phylogenetic analysis demonstrated close ancestry among SBEs, GOs, and RHSs and other MIA oxidizing CYPs (Fig. 3). As eukaryotic CYPs are membrane-bound, microsomes (total yeast membranes) were isolated for enzymatic assays. All four enzymes could convert 19*E*-geissoschizine with $[M+H]^+$ *m/z* 353 into a broadly eluting compound of *m/z* 351 (Fig. 4a). The broad peak was likely a result of conformer exchange and enol-keto resonance, similar to the substrate 19*E*-geissoschizing itself in our LC system (Fig. 2b). Tandem mass spectrometry (MS/MS) confirmed sarpagan bridge formation with characteristic daughter ion *m/z* 166 when compared with authentic polyneuridine aldehyde standard from the Evanno group (Fig 4a, Supplementary fig. 1). [2,10] Despite exhibiting identical LC-MS/MS profiles, the broad-eluting behavior was unable to distinguish between the polyneuridine aldehyde and akuammidine aldehyde epimers. In addition to the cyclized aldehyde, a further oxidized but not cyclized byproduct with *m/z* 349 (Fig. 4a) was tentatively identified as 3,4,5,6-dehydrogeissoschizine, based on its nearly identical UV absorption profile with that of serpentine (3,4,5,6-dehydroajmalicine, Supplementary fig. 1). Such UV profile is indicative of fully aromatized, beta-carboline structure, which is different from the profile of indole at 280 nm absorption maxima.

Solid polyneuridine aldehyde is stable yet it readily degrades in solution. [28,29] While it has been frequently described in literature, its NMR spectroscopic study was achieved only once by the Evanno group, by oxidizing quebrachidine to polyneuridine aldehyde and quickly analysing it in deuterated DMSO. [29] Akuammidine aldehyde, however, has not been studied by NMR. Due to the instability issue, enzymatically produced sarpagan bridge products have never been properly examined. Instead, their identity has been indirectly inferred by their conversions into downstream MIAs, such as vinorine via polyneuridine aldehyde esterase (PNAE) and vinorine synthase (VS), [2,10,38–41] or vellosimine and tombozine (both with inverted 16*S* stereochemistry) by total *R. serpentina* total proteins (Fig. 1). [42,43]

Due to the instability of the aldehyde and the scale of in vitro assays, we studied the aldehyde stereochemistry by $NaBH_4$ reduction and compared the reduced alcohols to authentic akuammidine and polynuridine standards. The akuammidine standard was purified from *A. tabernaemontana* (Supplementary fig. 8) in this study and we confirmed the structure and C16 stereochemistry by NMR (Supplementary fig. 9-14). The H17, H5, and H15 correlations in NOESY spectra indicated its 16*S* stereochemistry. NMR experiments of polyneuridine acquired from the Evanno group, showed H17 correlation to H6, H14, and H15 in NOESY spectra, confirming the 16*R* stereochemistry (Supplementary fig. 15-20). [28,29] Additionally, the two alcohols could be easily distinguished through ^1H NMR in $CDCl_3$ by comparing their chemical shifts of carbomethoxy group (δ 2.94 ppm for akuammidine caused by strong indole shielding and δ 3.73 ppm for polyneuridine) and H5 (δ 3.06 for akuammidine and 4.27 for polyneuridine) (Table 2). When the $NaBH_4$ reduced products were compared with the two closely eluting

alcohol standards, it became clear that all four SBEs produced diastereomeric aldehydes (Fig. 4b). CrSBE and TeSBE produced approximately equal amounts of both aldehydes, while VmSBE and RsSBE2 produced significantly more polyneuridine aldehyde (Fig. 4b).

Identifying an akuammidine aldehyde reductase that does not act on polyneuridine aldehyde

Since akuammidine was purified from *A. tabernaemontana*, we suspected that reductases may be found in this plant and other MIA-producing plants for akuammidine aldehyde reduction. Therefore, we further included total leaf proteins of *A. tabernaemontana*, *C. roseus*, *T. elegans*, and *A. scholaris* in our SBE microsomal assays. Both *A. tabernaemontana* and *A. scholaris* leaf proteins could reduce the products from four SBEs to akuammidine but not polyneuridine (Fig. 4a). In fact, neither leaf proteins could reduce the polyneuridine aldehyde standard (Fig. 4b), indicating that the unidentified reductase has a strict substrate preference for the 16*S* akuammidine aldehyde.

To date, two aldehyde reductases have been characterized for MIA biosynthesis. CrRedox2 reduces the stemmadenine aldehyde to its alcohol form stemmadenine.[6] Its homolog in *A. scholaris*, namely the rhazimal reductase AsRHR1/2 sharing 82% and 77% amino acid identity respectively with CrRedox2, reduce rhazimal to rhazimol. [11] We suspect that the putative akuammidine aldehyde reductase (AAR) activities in *A. scholaris* and *A. tabernaemontana* were contributed by homologous aldehyde reductases. We searched the *A. tabernaemontana* leaf transcriptome and identified two AAR candidates. One of the two purified, his-tagged proteins (Supplementary fig. 21) successfully reduced SBE products to akuammidine, while showing no activity with polyneuridine aldehyde (Fig. 4a and b). We therefore named this enzyme AtaAAR, which shared 85% amino acid identity with CrRedox2. The identification of AtaAAR therefore explained the formation of akuammidine in *A. tabernaemontana*. The results once again confirmed that diastereomeric aldehydes were produced by the four SBEs, as AtaAAR exclusively reduced akuammidine aldehyde to akuammidine.

Promiscuous Akuammidine/polyneuridine aldehyde deformylase converts both aldehydes to a single product pericyclivine

Instead of exhibiting akuammidine aldehyde reduction activity, *C. roseus* and *T. elegans* leaf proteins deformylated the SBE products to pericyclivine (Fig. 4a). In the absence of plant leaf proteins, SBE microsomes also produced a minor by-product isomeric to pericyclivine (*m/z* 323) with a slightly delayed elution time (Fig. 4a). The identity of this compound could not be determined due to the scale of the in vitro assays. However, its nearly identical MS/MS fragmentation pattern (daughter ion 166, Supplementary Fig. 1) suggested a close structural relationship to pericyclivine and other sarpagan alkaloids.

Unexpectedly, the *C. roseus* and *T. elegans* leaf proteins also transformed pure polyneuridine aldehyde to pericyclivine, despite its opposing C16 stereochemistry (Fig. 4c). This surprising result suggested that the unidentified deformylation reaction involves a sequence of C5-C16 sarpagan bridge opening, deformylation, and a stereospecific ring closure to reform the sarpagan bridge. This reaction ultimately produces pericyclivine with the akuammidine stereochemistry,

unifying both 16*S* and 16*R* aldehyde epimers into a single product. Pericyclivine is subsequently transformed into naturally occurring perivine in *C. roseus* (Fig. 2b, c) and the widely distributed MIA vobasine in *T. elegans*. [26] This unified activity also explains the absence of 16*R*-sarpagan MIAs in these two species.

Polyneuridine aldehyde esterase acts on both akuammidine/polyneuridine aldehydes to produce vellosimine C16-epimers

In *C. roseus* and *T. elegans*, the deformylation reaction joins sarpagan MIA biosynthesis from both akuammidine and polyneuridine aldehyde epimers. Interestingly, the Stoickgt group previously reported that the *R. serpentina* polyneuridine aldehyde esterase (RsPNAE) catalyzes the decarbomethoxylation of both polyneuridine and akuammidine aldehyde (Fig. 1). [43,44] While the fate of akuammidine aldehyde in this reaction was not further explored, the group indicated that short incubation of polyneuridine aldehyde with PNAE predominantly yielded 16-epi-vellosimine, which retains the same stereochemistry with the polyneuridine aldehyde precursor. Prolonged incubation resulted in the spontaneous epimerization of 16-epi-vellosimine to vellosimine. These epimers were distinguished by comparing the NMR chemical shifts of their aldehyde groups.

To elucidate the products of the akuammidine aldehyde-PNAE reaction and further investigate the fate of sarpagan C16 stereochemistry, we repeated these experiments using purified RsPNAE (Supplementary fig. 21) on both pure polyneuridine aldehyde and SBE products. Within just 1 minute of incubation with RsPNAE, polyneuridine aldehyde was converted to vellosimine epimers (*m/z* 293, Supplementary fig. 1), with the earlier-eluting epimer accumulating in greater quantity (Fig. 5). Prolonged incubation (80 minutes) resulted in the gradual epimerization of the earlier-eluting epimer into the later-eluting epimer, consistent with the Stoickgt group's findings. We identified the earlier-eluting epimer as 16-epi-vellosimine and the later-eluting epimer as vellosimine based on Stoickgt's assignment.

When the products of four SBE, containing a mixture of both aldehyde epimers, were subjected to PNAE assays, both vellosimine epimers were again quickly formed in just a minute (Fig. 5). Over the course of 80 minutes, spontaneous epimerization led to increased accumulation of vellosimine. This data complemented the previously missing experiment on akuammidine aldehyde decarbomethoxylation, demonstrating that aldehydes with both C16 stereochemistry contribute to downstream sarpagan MIA formation, including ajmaline, which is derived from 16-epi-vellosimine (Fig. 1).

Additionally, both vellosimine epimers were further reduced by total leaf proteins from *A. scholaris* and *A. tabernaemontana*, as well as the newly identified AtaAAR, to produce their corresponding alcohols (Fig. 5). Reducing the epimers with $NaBH_4$ produced identical results (Fig. 5). Vellosimine-reducing activity has also been previously documented from *R. serpentina* cell cultures.[43] Out of the two alcohol epimers, tombozine, bearing the akuammidine stereochemistry, can undergo additional hydroxylation at C10 to form sarpagine, which is a widely distributed MIA in Apocynaceae. [43] The spontaneous epimerization of 16-epi-vellosimine to vellosimine evidently contributed to tombozine becoming the predominant alcohol product.

Rhazimal synthases from three species produce strictly 16*R* product

Oxidative C7–C16 cyclization of 19*E*-geissoschizine theoretically produces rhazinaline (16*S*), reported in *Rhazya stricta* [21] and rhazimal (16*R*). Rhazimal synthase (RHS) was first identified and characterized in *Alstonia scholaris*. Sharing 62% amino acid identity with CrGO, AsRHS generates both rhazimal and preakuammicine aldehyde iminium, with the latter spontaneously deformylating to akuammicine (Fig. 1). These findings were recently corroborated by the characterization of several AsRHS variants in *A. scholaris.* [45] The C16 stereochemistry of AsRHS products was confirmed by reducing the products to their corresponding alcohols and comparing them with a chemically synthesized rhazimol standard. [11,30]

To further investigate the natural occurrence of these compounds, we purified rhazimal directly from *A. tabernaemontana* leaves (Supplementary Fig. 8) and confirmed its structure and 16*R* stereochemistry using NMR (Supplementary Fig. 22–27). NOESY spectra revealed correlations between H17 and H15, H14, and indole H9, consistent with the 16*R* configuration. Instead of rhazimal, we found and purified strictamine from *V. minor* leaves, which derives biosynthetically from rhazimal deformylation, (Supplementary Fig. 28–33). Similar to rhazimal, the H16 correlations with H15, H14, and indole H9 confirmed the 16*R* stereochemistry of strictamine, confirming its intermediacy from rhazimal. These findings suggested that akuammiline type MIA biosynthesis occurs in both *A. tabernaemontana* and *V. minor*.

Using the *A. scholaris* RHS sequence as a reference, we searched transcriptomes from *A. tabernaemontana* and *V. minor* and identified two new RHS orthologs AtaRHS and VmRHS, which share 84% and 74% amino acid identity with AsRHS, respectively. Given the phylogenetic proximity of *A. tabernaemontana* and *R. stricta*, AtaRHS might produce both rhazimal epimers. To test this, we expressed AsRHS, AtaRHS, and VmRHS in baker's yeast. Microsomes containing these enzymes oxidized 19*E*-geissoschizine to both rhazimal and akuammicine, as confirmed by LC-MS/MS comparison with authentic standards (Fig. 6). Notably, we observe no evidence of a rhazimal 16-epimer for any of the three enzymes. The akuammicine standard was isolated from a *C. roseus* mutant that accumulates significant quantities of this compound, with its structure previously verified by NMR. [6,46]

Given that several Apocynaceae plants exhibit deformylation activity on akuammidine/polyneuridine aldehydes, it is plausible that some species may possess rhazimal deformylase to produce strictamine. Consistent with this hypothesis, we found that the total leaf proteins from *V. minor* and A. *scholaris* could deformylate rhazimal to strictamine (Fig. 6), providing a biochemical explanation for the biosynthesis of strictamine in *V. minor*. In contrast, *A. tabernaemontana* leaf proteins and *C. roseus* leaf proteins lacked deformylation activity, consistent with the observed accumulation of rhazimal but not strictamine in *A. tabernaemontana* (Supplementary fig. 8). Additionally, we discovered that leaf proteins from *A. scholaris* and *C. roseus* could reduce rhazimal to rhazimol, which co-eluted with the alcohol generated by $NaBH_4$ reduction (Fig. 6). These findings further confirmed the absence of rhazinaline biosynthesis activity of the three tested RHS enzymes, while validating the presence of reductase and deformylase activities in Apocynaceae plants, which together facilitate the biosynthesis of rhazimol and strictamine.

Discussion

With the rapid advancement of plant transcriptome and genome sequencing at tissue and cellular levels, remarkable progress has been made in understanding monoterpene indole alkaloid (MIA) biosynthesis. The elucidation of the complete biosynthetic pathways for over 30 steps of anhydrovinblastine production *in C. roseus* and 20 steps of ajmaline biosynthesis in *R. serpentina* has provided a foundational framework for studying MIA biogenesis. [2,6,10,13–15,18,47–49] These breakthroughs have revealed the extraordinary enzymatic machinery responsible for the formation of the highly complex MIA skeletons.

MIA biosynthesis originates from the central precursor strictosidine. Reduction of strictosidine aglycone by cinnamyl alcohol dehydrogenase (CAD)-like reductases generates the corynanthe, yohimbine, and heteroyohimbine backbones, introducing multiple stereocenters in the process. [4,5,7,8] This critical diversification step is further enhanced by three major cyclization events catalyzing the formation of corynanthe-type MIA 19*E*-geissoschizine. The activities of homologous CYPs, geissoschizine oxidase (GO), sarpagan bridge enzyme (SBE), and rhazimal synthase (RHS), convert geissoschizine into strychnos, sarpagan, and akuammiline skeletons. [6,10,11] Subsequent modifications and structural decorations generate additional MIA types, such as iboga, aspidosperma, pseudoaspidosperma, and ajmalan, resulting in over 3,000 structurally diverse MIAs.

In this study, we investigated the stereochemical and mechanistic outcomes of geissoschizine cyclization mediated by SBE and RHS, using two previously characterized CYPs and five novel CYPs derived from six Apocynaceae species. Notably, the stereochemistry of the SBE products had remained elusive due to the instability of the intermediates. Our results demonstrated that SBEs from *C. roseus*, *T. elegans*, *V. minor*, and *R. serpentina* produce diastereomeric akuammidine aldehyde (16*S*) and polyneuridine aldehyde (16*R*) at varying ratios (Fig. 4a-b). This conclusion was supported by the reduction of these aldehydes into two stereochemically distinct alcohols using $NaBH_4$ and the discovery of a new akuammidine aldehyde reductase (AAR) that selectively reduces akuammidine aldehyde but not polyneuridine aldehyde (Fig. 4b). NMR characterization of these products allowed us to definitively establish the stereochemistry of the SBE reaction.

The identification of akuammidine aldehyde as a product of SBE catalysis provided a mechanistic explanation for the natural accumulation of sarpagan MIAs, such as akuammidine, pericyclivine, perivine, and vobasine with this stereochemistry, across Apocynaceae species. However, the diastereomeric nature of SBE catalysis raised questions about the metabolic fate of polyneuridine aldehyde in sarpagan-accumulating species like *C. roseus* and *T. elegans*, which exclusively produce MIAs with the akuammidine stereochemistry. [6,26] We resolved this discrepancy by identifying deformylase activity in the leaf proteins of these species. Unifying the biosynthesis, this unidentified deformylase converts both akuammidine and polyneuridine aldehyde into a single product, pericyclivine, bearing the akuammidine stereochemistry (Fig. 4a, c). It is likely that this reaction involves the formation of a Schiff base at *N*4, followed by a stereospecific ring closure that restores the sarpagan bridge with a defined stereochemistry.

The physiological relevance of CrSBE *in planta* was validated using virus-induced gene silencing (VIGS) in *C. roseus* leaves. To redirect metabolic flux toward the otherwise suppressed sarpagan MIAs, we silenced CrGO, the major competitor of CrSBE for 19*E*-geissoschizine substrate. In this background, silencing CrSBE significantly reduced the accumulation of pericyclivine and perivine, confirming CrSBE's *in planta* role in sarpagan biosynthesis (Fig 2a-c).

We also revisited the decarbomethoxylation reaction of akuammidine and polyneuridine aldehydes by RsPNAE, which was previously poorly characterized. Our findings demonstrated that RsPNAE processes both aldehydes, yielding 16-epi-vellosimine and vellosimine as a diastereomeric mixture (Fig. 5). Over time, 16-epi-vellosimine spontaneously epimerized to vellosimine (Fig. 5). The acetylation of 16-epi-vellosimine by vinorine synthase allows its entry into the ajmaline biosynthetic pathway, while both epimers can be reduced by AtaAAR to form 16-epi-tombozine and tombozine. The latter undergoes 10-hydroxylation to yield sarpagine, a widely distributed MIA (Fig. 1).

In the case of RHS-mediated C7-C16 cyclization, we demonstrated that RHS enzymes *from A. scholaris, A. tabernaemontana*, and *V. minor* exclusively produce rhazimal (16R), not its epimer rhazinaline (16S). We verified the stereochemistry by direct rhazimal NMR analysis. This strict stereochemical control is consistent with CrGO [6,15] , distinguishing these enzymes from SBEs, which exhibit weak stereochemical selectivity. Although *A. tabernaemontana* is closely related to *R. stricta*, which reportedly produces rhazinaline, [21] its RHS did not show any evidence of rhazinaline production. It remains possible that *R. stricta* contains an epimerase or that its RHS produces both C16 diastereomers.

Additionally, we identified deformylase activity in the leaf proteins of *V. minor* and *A. scholaris*, which deformylated rhazimal to strictamine (Fig. 4a). Although the rhazimal deformylase and the akuammidine/polyneuridine aldehyde deformylase share functional similarities, our results clearly indicated that they are distinct enzymes. Specifically, in our experiments, *C. roseus* leaf proteins demonstrated the ability to deformylate akuammidine and polyneuridine aldehyde epimers but showed no activity toward rhazimal (Fig. 4a, Fig. 6). Similarly, *A. scholaris* leaf proteins could deformylate rhazimal but not the akuammidine and polyneuridine aldehyde epimers (Fig. 4a, Fig. 6). The absence of rhazimal deformylase in *A. tabernaemontana* additionally explains the accumulation of rhazimal without strictamine. A recent study reported the spontaneous formation of strictamine during the AsRHS reaction. [45] However, under our experimental conditions, such spontaneous deformylation was negligible. The discrepancy is likely attributable to differences in reaction conditions, which may influence the stability of intermediates and the likelihood of spontaneous transformations.

In conclusion, this study provides mechanistic and stereochemical insights into SBE- and RHS-mediated cyclization reactions, deformylase, esterase, and reductase activities, and spontaneous transformations that underpin the extraordinary structural diversity of MIAs. These findings deepen our understanding of how unique enzyme activities in Apocynaceae species shape the biosynthesis and accumulation of MIAs, contributing to their ecological and pharmacological significance.

Material and Methods

Chemicals

Catharanthine, vindoline, and vindolinine standards were purchased from Sigma Aldrich (Millipore Sigma, Burlington, MA, USA). Perivine was purchased from AvaChem Scientific (San Antonio, TX, USA). Vindorosine and epi-vindolinine standards were previously purified from *C. roseus* plant. [13] 19*E*- and 19*Z*-geissoschizine were produced as previously described by reacting strictosidine aglycone produced by CrSTR and CrSGD with CrGS in vitro. [5] The ethyl acetate extracted products were dried under vacuum and purified by preparative thin layer chromatography (TLC, Silica gel 60 F254, Millipore Sigma, Burlington, MA, USA) and solvents toluene: ethyl acetate: methanol 15:4:1 (v:v:v). Both pericyclivine and akuammicine were purified from VIGS plants in previous studies and structurally confirmed by NMR. In this study, pericyclivine structure was confirmed again in $CDCl_3$ with NOESY. For alkaloids purified from plant materials, 50 or 100 g of *A. tabernaemontana* or *V. minor* leaves were extracted with ethyl acetate. The resulting extract was reduced in volume, and extracted by 1M HCl. The HCl extract was basified to pH 8 by NaOH and extracted by ethyl acetate to afford total alkaloids. *V. minor* alkaloids were separated by TLC with solvents ethyl acetate: methanol 9:1 (v:v). The band with Rf=0.09 was harvested and further separated on TLC with pure methanol to afford strictamine with Rf=0.47. *A. tabernaemontana* alkaloids were separated by TLC with solvents ethyl acetate: methanol 9:1 (v:v) to afford akuammidine and rhazimal.

Cloning

Full-length *CrSBE, VmSBE, VmRHS, AsRHS, AtaRHS, AtaAAR, RsPNAE,* and the VIGS fragment of *CrSBE* and *CrGO* were amplified from respective plant leaf cDNA using primers 1-18 (Supplementary table 1). Codon-optimized TeSBE was synthesized (Bio Basic, Markham, ON, Canada). VmRHS was cloned in pYES-DEST52 vector using Gateway® BP/LR clonases (ThermoFisher, Waltham, MA, USA) according to manufacture's protocol. All other CYPs were cloned in pESC-Leu vector containing CrCPR, within BamHI/SalI sites. RsPNAE and AtaAAR was cloned in pET30b+ vector within BamHI/SalI sites. For silencing CrSBE and CrGO with a single chimeric construct, the VIGS fragment of CrSBE was cloned in EcoRI site of pTRV2 vector and the VIGS fragment of CrGO was cloned within XhoI/XbaI sites. For single GO-silencing, a previous pTRV2-GO construct was used. [6] All CYPs were mobilized to *Saccharomyces cerevisiae* strain BY4741 (MATα his3Δ1 leu2Δ0 met15Δ0 ura3Δ0 YPL154c::kanMX4). AtaAAR and RsPNAE were mobilized to BL21DE3 *E. coli* for protein expression. The pTRV2 vectors were mobilized to *Agrobacterium tumefaciens* strain GV3101.

Virus-induced gene silencing

The VIGS experiments were carried out as described previously with a phytoene desaturase (PDS) silencing indicator. [6] In brief, cells from overnight cultures of *A. tumefaciens* carrying pTRV1 vector and various pTRV2 vectors grown at 28 °C shaking incubator were collected by centrifugation and resuspended in infection buffer (10 mM MES pH 5.6, 10 mM $MgCl_2$, 0.2 mM acetosyringone) to OD_{600} 1.5. The suspensions were incubated at 28 °C for 2.5 hr, then equal pTRV1 and pTRV2 suspensions were mixed just before the infection. A sharpened toothpick dipped in the mixed suspension was used to pierce just underneath the apical meristem of 4-week-old *C. roseus* cv. Pacifica XP White with 2-3 pairs of true leaves, then 0.1 mL suspension mixture was used to flood the wound. The infected plants were grown at a glasshouse with 18/6 hr photoperiod at 25 °C for approximately 4 weeks, when the VIGS-PDS leaves developed white

490 sectors. The developing leaves were cut in half along the main vertical vein. One half of the
491 leaves were used for RNA extraction and qPCR, whereas the other half leaves were ground and
492 extracted with methanol for alkaloid analysis using LC-MS/MS.
493
494 **cDNA synthesis and qRT-PCR**
495 Plant leaves (10-100 mg) were ground in liquid nitrogen using a small pestle and a microtube.
496 The total RNA were extracted with TRI Reagent™ (ThermoFisher, Waltham, MA, USA)
497 according to the manufacture's protocol. The cDNA was synthesized using the LunaScript® RT
498 SuperMix (New England Biolabs, Ipswich, MA, USA) according to the manufacture's protocol.
499 qRT-PCR experiments were performed on an Agilent AriaMx Real-Time PCR instrument using
500 the SensiFAST SYBR No-ROX qPCR 2X master mix (FroggaBio, Concord, Canada) according
501 to the manufacture's protocol. The qRT-PCR (10 µL, 5 ng total RNA) cycles included 40 cycles
502 of 95 °C for 10 s and 58 °C for 30 s. The Ct values and standard ΔΔCt method was used to
503 quantify gene expression levels, which are normalized by using the expression of C. roseus 60S
504 ribosomal RNA housekeeping gene. [5,13] The changes of gene expression levels were evaluated by
505 two-tailed, unpaired Student-t test from 7 independent biological samples with 3 technical
506 replicates using Microsoft Excel.
507
508 **Yeast microsome isolation**
509 Overnight culture (1 mL) of yeast was used to inoculate 100 mL SC-Leu medium with 2%
510 glucose. The yeast was grown at 30°C for 24 h. The harvested cells were lysed in TES buffer (10
511 mM Tris-HCl pH 7.5, 1 mM EDTA, 0.6 M sorbitol) with glassbeads at 30 Hz, 3 min duration,
512 and four times at 4°C using a Beadbug® homogenizer (Benchmark Scientific, Sayreville, NJ,
513 USA). The lysate was centrifuged at 8,000 g for 10 min at 4°C, and the supernatant was further
514 centrifuged at 100,000 g for 1 hr at 4 °C to pellet microsomes. The microsomes were suspended
515 in TEG buffer (10 mM Tris-HCl pH 7.5, 1 mM EDTA, and 10% (v/v) glycerol) and stored in -
516 80°C.
517
518 ***E. coli* protein purification**
519 LB media (200 mL) were first inoculated with 2 ml overnight *E. coli* BL21-DE3 cultures
520 harboring various genes, then grown to OD_{600} 0.6-0.7 at 37 °C. The cultures were induced with
521 0.1 mM IPTG at 15 °C overnight. The harvested cells were sonicated in lysis buffer (20 mM
522 Tris-HCl pH 7.5, 100 mM NaCl, 10 mM imidazole, 10% (v/v) glycerol). After centrifugation at
523 10,000 g for 10 min, the supernatants were incubated with 1 ml Ni- NTA resin at 4°C for 20 min.
524 The resins were washed with 20 ml wash buffer (20 mM Tris-HCl pH 7.5, 200 mM NaCl, 30
525 mM imidazole, 10% (v/v) glycerol). The recombinant proteins were eluted with elution buffer
526 (20 mM Tris-HCl pH 7.5, 100 mM NaCl, 250 mM imidazole, 10% (v/v) glycerol), desalted into
527 20 mM Tris-HCl pH 7.5, 100 mM NaCl, 10% (v/v) glycerol, and stored at -80°C.
528
529 **In vitro assay**
530 Standard yeast microsome assays (100 µL) included 20 mM Tris-HCl pH 7.5, 100 ng
531 geissoschizine, 1 mM NADPH, 50 µg yeast microsomal proteins, 1 µg *E. coli* recombinant
532 proteins, and/or 20 µg plant total proteins. The reaction took place at 30 °C for 1 hr unless
533 otherwise noted. The reaction was mixed with equal volume of methanol, centrifuged, and filtred
534 for LC-MS/MS analysis.
535

LC-MS/MS and NMR

The samples were analyzed by Ultivo Triple Quadrupole LC-MS/MS system from Agilent (Santa Clara, CA, USA), equipped with an Avantor® ACE® UltraCore C18 2.5 Super C18 column (50×3 mm, particle size 2.5 μm) as well as a photodiode array detector and a mass spectrometer. The following solvent systems were used: Solvent A, Methanol: Acetonitrile: Ammonium acetate 1 M: water at 29:71:2:398; solvent B, Methanol: Acetonitrile: Ammonium acetate 1 M: water at 130:320:0.25:49.7. The following linear elution gradient was used: 0-5 min 80% A, 20% B; 5-5.8 min 1% A, 99% B; 5.8-8 min 80% A, 20% B; the flow during the analysis was constant and 0.6 ml/min. The photodiode array detector range was 200 to 500 nm. The mass spectrometer was operated with the gas temperature at 300°C and gas flow of 10 L/min. Capillary voltage was 4 kV from m/z 100 to m/z 1000 with scan time 500 ms and the fragmentor performed at 135 V with positive polarity. The MRM mode was operated as same as scan mode with the adjusted precursor and product ion. NMR spectra were recorded on an Agilent 400 MR, a Bruker Avance III HD 400 MHz, or a Bruker Avance AV I 600 digital NMR spectrometer in acetone-*d6* or $CDCl_3$.

Acknowledgements

We would like to express our sincere gratitude to Prof. Laurent Evanno at the Université de Paris-Sud for generously providing the polyneuridine aldehyde and alcohol standards. This research is supported by a Natural Sciences and Engineering Research Council of Canada (NSERC) Discovery Grant and a New Brunswick Innovation Foundation (NBIF) Research Assistantship Initiative Grant to Y.Q.

Conflict of interest

The authors declare that there are no conflicts of interest.

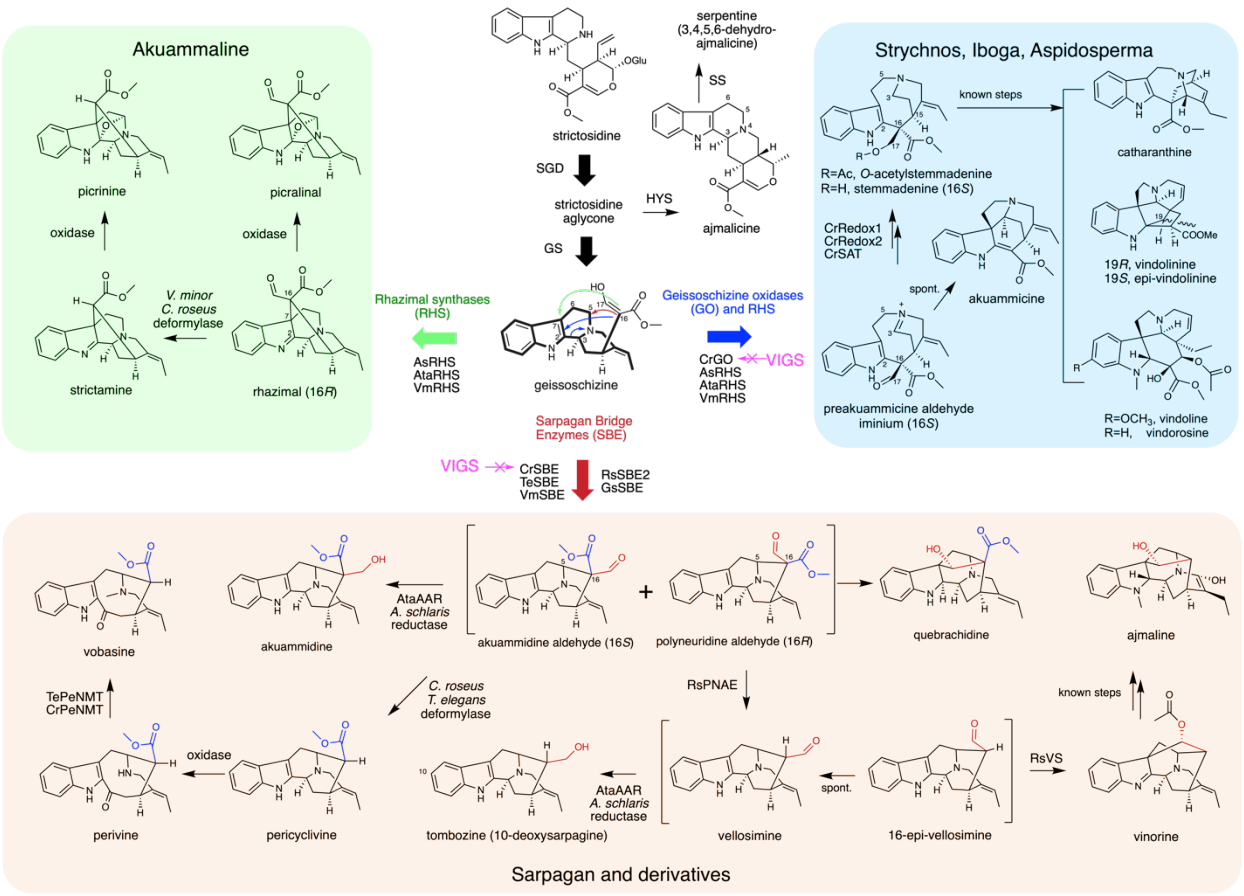

Figure 1. The biosynthetic framework of monoterpenoid indole alkaloids (MIAs) for akuammiline, sarpagan, strychnos, iboga and aspidosperma types. 19E-geissoschizine cyclizations by homologous cytochrome P450 monooxygenases (CYPs) play a pivotal role in producing these major MIA skeletons.

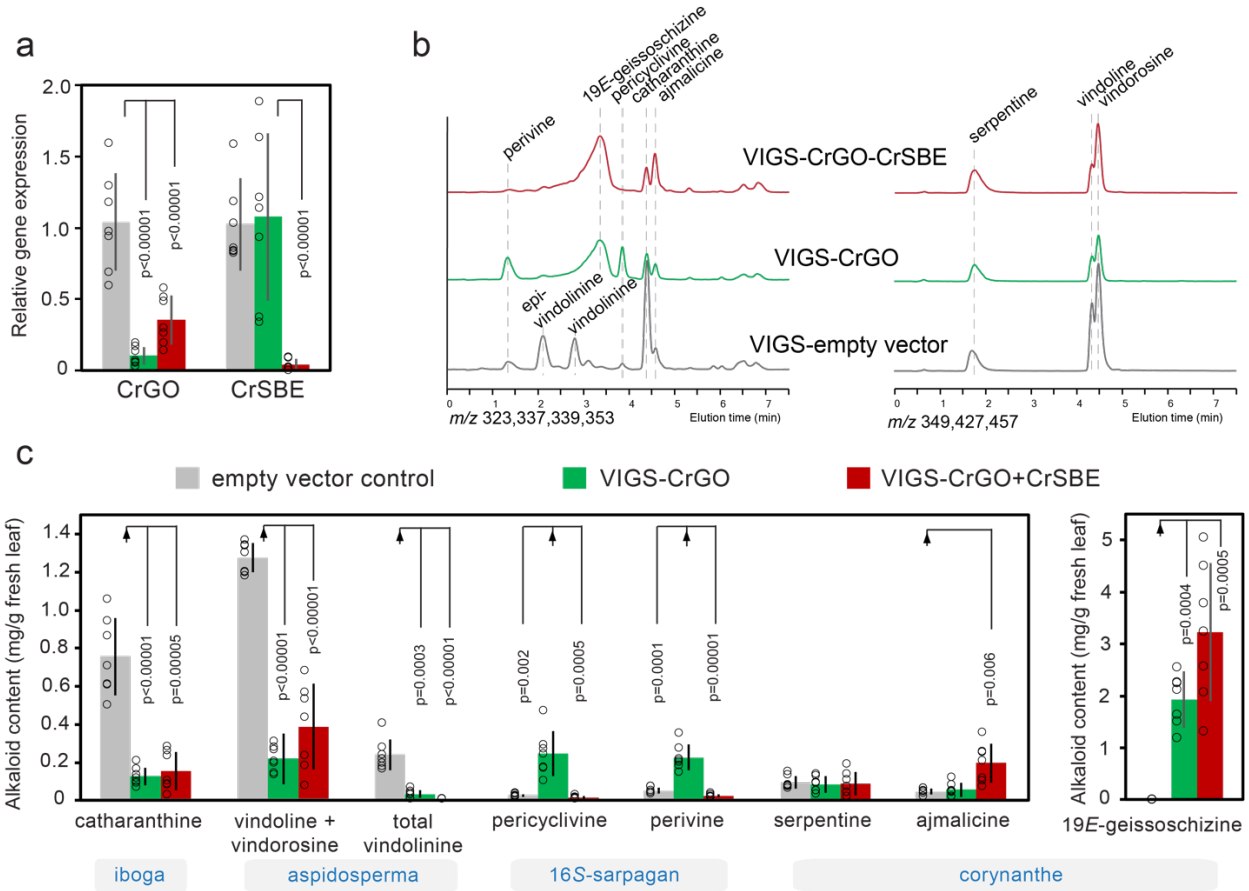

Figure 2. Virus-induced gene silencing (VIGS) of CrSBE significantly reduced sarpagan alkaloid accumulation in *C. roseus* leaf. Co-silencing CrGO redirected metabolic flux to the sarpagan biosynthetic pathway, enabling proper evaluation of CrSBE's physiological role. (a) qRT-PCR analysis of the relative expression levels of CrGO and CrSBE in the empty vector control, VIGS-CrGO, and VIGS-CrGO+CrSBE co-silencing plants. (b) Representative LC-MS chromatograms for selected ions $[M+H]^+$ *m/z* 323,337,339,349,353,427,457 show the reduction and increase of alkaloids in control and VIGS plants. (c) Quantification of major alkaloids in control and VIGS plants. Data was generated from seven independent plants per treatment. Individual data points are shown as circles, and error bars represent standard deviation. Statistical analysis was performed using the Student's *t*-test. The structures of alkaloids are found in Figure 1.

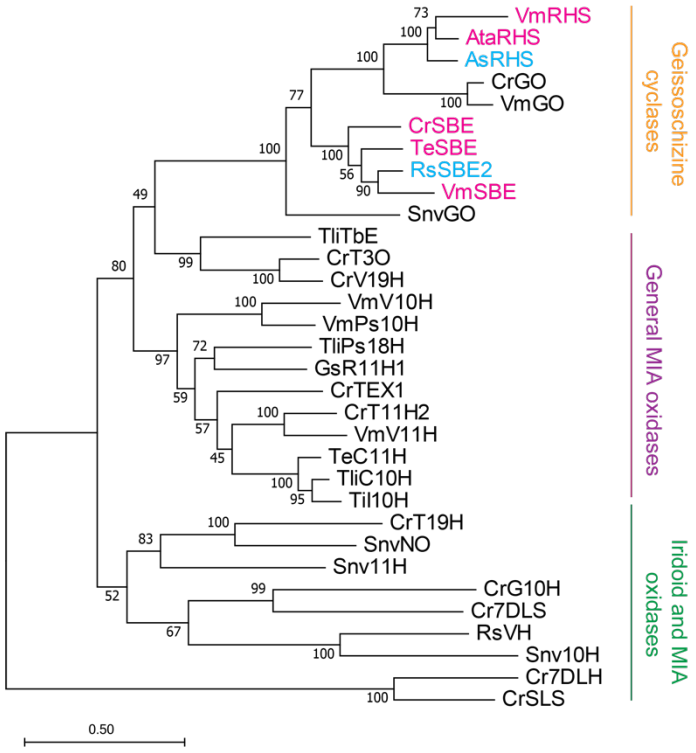

Figure 3. Phylogenetic analysis of geissoschizine oxidases (GOs), sarpagan bridge enzymes (SBEs), rhazimal synthases (RHSs), and other characterized cytochrome P450 monooxygenases (CYPs) involved in MIA biosynthesis. Newly identified and characterized enzymes from this study are highlighted in red, while previously characterized RHS and SBE enzymes are marked in blue. Evolutionary analyses were conducted in MEGA11. The evolutionary history was inferred by using the Maximum Likelihood method and JTT matrix-based model. The tree with the highest log likelihood is shown. The percentage of trees in which the associated taxa clustered together is shown next to the branches (100 bootstrap replicates). Initial tree(s) for the heuristic search were obtained automatically by applying Neighbor-Join and BioNJ algorithms to a matrix of pairwise distances estimated using the JTT model, and then selecting the topology with superior log likelihood value. The tree is drawn to scale, with branch lengths measured in the number of substitutions per site (scale bar). As: *Alstonia scholaris*; Ata: *Amsonia tabernaemontana*; Cr: *Catharanthus roseus*; Gs: *Gelsemium sempervirens*; Snv: *Strychnos nux-vomica*; Rs: *Rauvolfia serpentina*; Te: *Tabernaemontana elegans*; Tli: *Tabernaemontana litoralis*; Ti: *Tabernanthe iboga*; Vm: *Vinca minor*; R11H1: rankinidine 11-hydroxylase 1; Ps18H: pseudovincadifformine 18-hydroxylase; I10H: ibogamine 10-hydroxylase; T16H2, tabersonine 16-hydroxylase 2; TEX1: tabersonine 14,15-α-epoxidase; TbE: tabersonine 14,15-β-epoxidase; T3O: tabersonine 3-oxidase; V19H: (+)-vincadifformine 19-hydroxylase; Snv10H: strychnine 10-hydroxylase; Snv11H: β-colubrine 11-hydroxylase; NO: norfluorocurarine 18-hydroxylase; T19H: tabersonine 19-hydroxylase; VH: vinorine hydroxylase; 7DLH: 7-deoxyloganic acid hydroxylase; SLS: secologanine synthase.

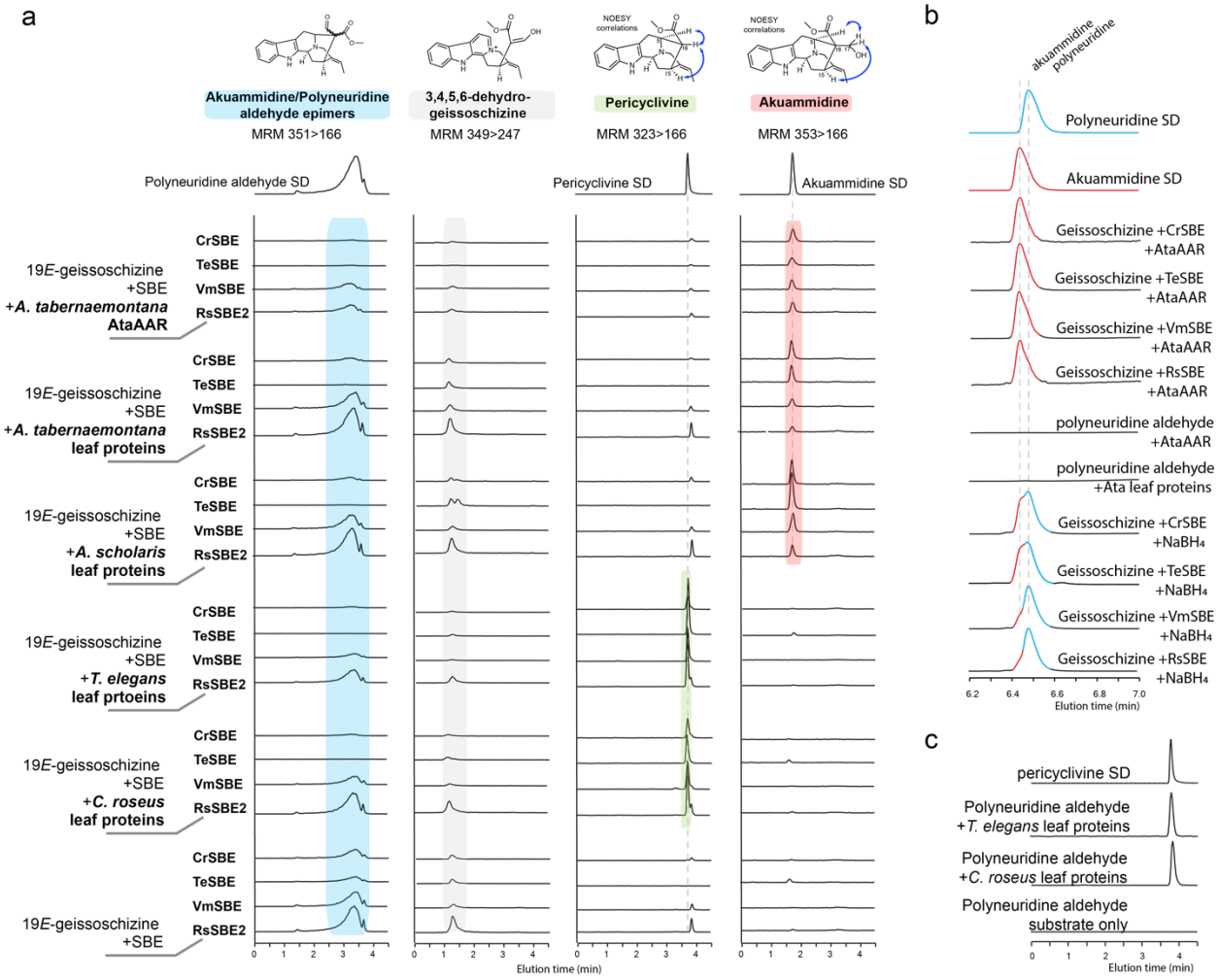

Figure 4. Sarpagan bridge enzymes (SBEs) from *C. roseus*, *T. elegans*, *V. minor*, and *R. serpentina* catalyze the in vitro production of diastereomeric akuammidine aldehyde (16*S*) and polyneuridine aldehyde (16*R*) from 19*E*-geissoschizing, which are subsequently converted enzymatically to akuammidine and pericyclivine by species-specific enzyme activities. (a) SBEs from the four species converted 19*E*-geissoschizine substrate into a mixture of akuammidine/polyneuridine aldehyde epimers and a byproduct 3,4,5,6-dehydrogeissoschizine. Total leaf proteins of *C. roseus* and *T. elegans* deformylated both aldehyde epimers to a single product pericyclivine, while total leaf proteins of *A. scholaris* and *A. tabernaemontana* instead reduced akuammidine aldehyde to akuammidine. The LC-MS/MS chromatograms show multiple reaction monitoring (MRM) transitions using parameters $[M+H]^+$ *m/z* 351>166 for the aldehydes, *m/z* 349>247 for 3,4,5,6-dehydrogeissoschizine, *m/z* 323>166 for pericyclivine, and *m/z* 353>166 for akuammidine and polyneuridine. The MS/MS spectra for these alkaloids are shown in Supplementary figure 1. (b) $NaBH_4$ reduction of SBE products generated both akuammidine and polyneuridine epimers, confirming their diastereomeric nature. However, total plant leaf proteins and AtaAAR showed specificity for akuammidine aldehyde reduction, with no activity on polyneuridine aldehyde. (c) Pure polyneuridine aldehyde was deformylated by *C. roseus* and *T. elegans* leaf proteins to form pericyclivine with opposing C16-stereochemistry.

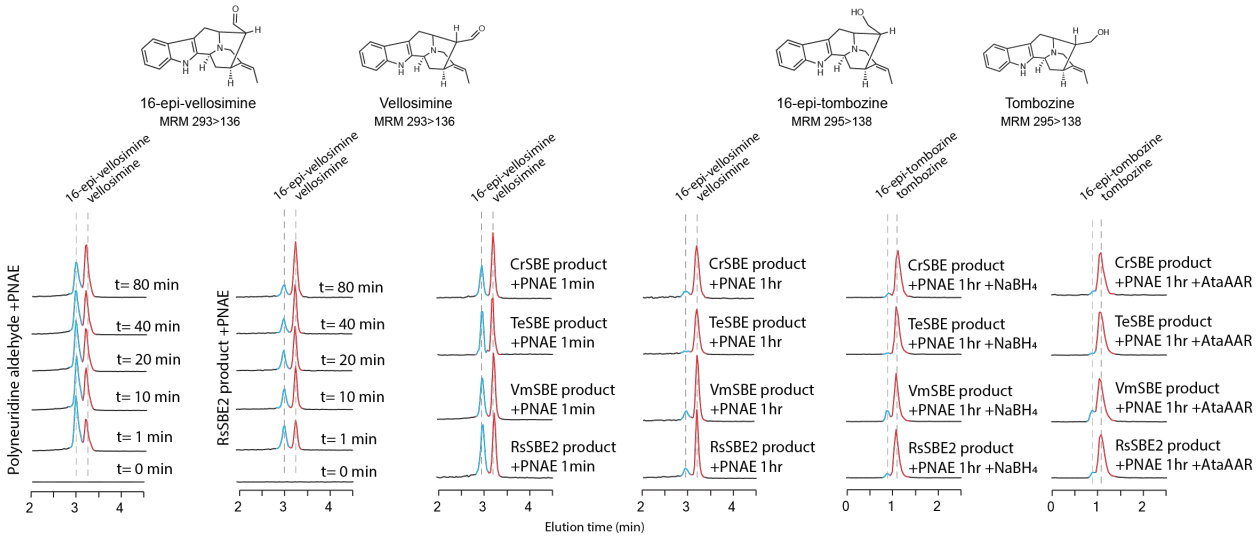

Figure 5. The polyneuridine aldehyde esterase (PNAE) catalyzes the decarbomethoxylation of both akuammidine aldehyde and polyneuridine aldehyde, producing a mixture of vellosimine C16-epimers, which are subsequently reduced to their corresponding alcohols by akuammidine aldehyde reductase (AtaAAR). The two left panels display the time course of the PNAE reaction with pure polyneuridine aldehyde and the akuammidine/polyneuridine aldehyde mixture produced by RsSBE2. The middle two panels show the PNAE reaction with products from four SBEs at 1 min and 1 hr. The spontaneous epimerization of 16-epi-vellosimine to vellosimine is evident in these reactions. The final two panels demonstrate that AtaAAR reduces both vellosimine epimers to their corresponding alcohols, 16-epi-tombozine and tombozine. Treatment of the vellosimine epimers with $NaBH_4$ yielded identical results. The LC-MS/MS chromatograms show multiple reaction monitoring (MRM) transitions using parameters $[M+H]^+$ *m/z* 293>136 for vellosimine epiemrs and *m/z* 295>138 for tombozine epimers. The MS/MS spectra for these alkaloids are shown in Supplementary figure 1.

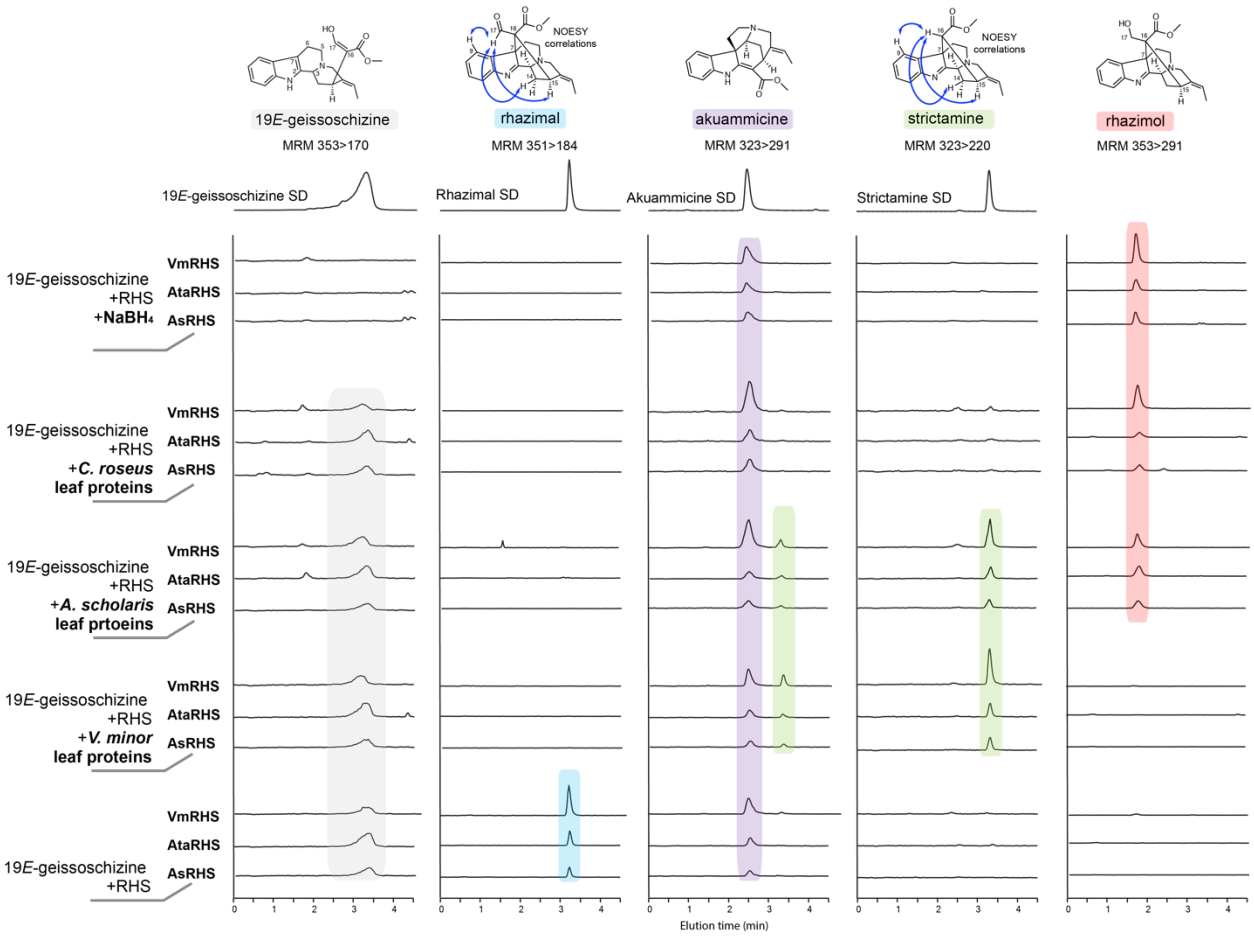

Figure 6. Rhazimal synthases (RHSs) from *A. scholaris*, *A. tabernaemontana*, and *V. minor* catalyzed in vitro production of rhazimal (16*R*) but not rhazinaline (16S) from 19*E*-geissoschizine, which are subsequently converted enzymatically to rhazimol and strictamine by species-specific enzyme activities. RHSs also generated significant amounts of akuammicine. Total leaf proteins of *V. minor* deformylated rhazimal to strictamine preserving the C16 stereochemistry. In contrast, total leaf proteins of *C. roseus* reduced rhazimal to rhazimol while *A. scholaris* leaf proteins exhibited dual activity, producing both strictamine and rhazimol simultaneously. $NaBH_4$ reduction of RHS products yielded a single product rhazimol, further confirming rhazimal's stereochemical identity. The LC-MS/MS chromatograms show multiple reaction monitoring (MRM) transitions using parameters $[M+H]^+$ *m/z* 353>170 for geissoschizine, *m/z* 351>184 for rhazimal, *m/z* 323>291 for akuammicine, *m/z* 323>220 for strictamine, and *m/z* 353>291for rhazimol. Strictamine also exhibits m/z 323 > 291 ion transitions, which are observed alongside those of akuammicine in the same chromatograms. The MS/MS spectra for these alkaloids are shown in Supplementary figure 1.

Table 1. ^{13}C NMR chemical shifts of alkaloids in this study

	Akuammidine		Polyneuridine			Pericyclivine		Rhazimal	Strictamine
	This study	Ref [50]	This study	Ref [50]	Ref [6]	This study	Ref [50]	This study	This study
	$CDCl_3$	$CDCl_3$	$CDCl_3$	$CDCl_3$	acetone-*d*6	$CDCl_3$	$CDCl_3$	$CDCl_3$	$CDCl_3$
NH	7.75 br s	7.90 br s	7.77 br s	7.81 br s	9.87 br s	7.73 br s	7.78 br s	-	-
3	4.23 d	4.24 br d	4.07 dd	4.06 dd	4.20 br d	4.23 d	4.21 br d	4.62 d	4.68 d
5	3.06 d	3.1 m	4.27 d	4.27 br d	3.69 ddd	3.68 ddd	3.68 ddd	2.62 ddd 2.67 ddd	2.59 ddd 2.71 ddd
6	2.91 dd 3.29 dd	2.94 dd 3.30 dd	2.94 dd 3.10 dd	2.94 br d 3.10 dd	2.80 m 3.20 dd	2.91 dd 3.24 dd	2.91 dd 3.24 dd	2.12 dd 3.85 ddd	1.99 dd 3.74 ddd
9	7.43 d	7.42 d	7.49 d	7.48 d	7.40 d	7.41 d	7.41 d	7.56 d	7.42 d
10	7.05 dt	7.05 dt	7.10 dt	7.10 dt	6.98 dt	7.04 dt	7.04 dt	7.22 dt	7.16 dt
11	7.11 dt	7.11 dt	7.15 dt	7.15 dt	7.05 dt	7.11 dt	7.10 dt	7.37 dt	7.33 dt
12	7.28 d	7.28 d	7.31 d	7.31 dd	7.33 d	7.29 d	7.28 d	7.63 dt	7.62 d
14	1.86 dd 2.66 dd	1.85 dd 2.67 dd	1.88 m 1.90 ddd	1.85 ddd 1.91 ddd	1.74 dddd 2.63 ddd	1.78 dddd 2.59 ddd	1.76 ddd 2.58 ddd	2.19 dd 2.49 dddd	1.74 dd 2.68 dddd
15	3.06 d	3.1 m	3.21 t	3.21 dd	2.96 br s	2.99 br t	2.98 m	3.83 br s	3.50 br s
16	-	-	-	-	2.83 m	2.82 dd	2.82 dd	-	2.08 d
17	3.68 d 3.83 d	3.67 d 3.83 d	3.62 d 3.71 d	3.61 d 3.71 d	-	-	-	8.51 s	-
18	1.65 dt	1.65 ddd	1.60 dt	1.60 br d	1.65 ddd	1.62 dt	1.62 ddd	1.60 dd	1.55 dd
19	5.41 q	5.39 br q	5.28 qt	5.28 br q	5.28 q	5.27 tq	5.27 br q	5.51 q	5.50 q
21	3.60 dd 3.61 dt	3.58 def 3.58 def	3.60 m 3.65 m	3.6 m 3.6 m	3.60 m 3.60 m	3.64 t 3.64 t	3.6 m 3.6 m	3.15 d 4.12 d	3.11 d 4.06 dt
OCH_3	2.94 s	2.94 s	3.73 s	3.73 s	3.10 s	3.06 s	3.75 s	3.81 s	3.72 s

Table 2. ^{1}H NMR chemical shifts of alkaloids in this study

	Akuammidine		Polyneuridine		Pericyclivine			Rhazimal		Strictamine	
	This study	Ref [50]	This study	Ref [50]	Ref	This study	Ref [50]	This study	Ref [51]	This study	Ref [51]
	$CDCl_3$	$CDCl_3$	$CDCl_3$	$CDCl_3$	acetone-*d*6	$CDCl_3$	$CDCl_3$	$CDCl_3$	$CDCl_3$	$CDCl_3$	$CDCl_3$
2	137.4	136.6*	137.09	136.2*	138.8	137.5	136.6*	189.4	190.50 weak	191.4	190.98
3	50.7	51.4	49.14	49.0	50.0	50.6	50.4	54.8	54.70	55.2	55.15
5	58.1	58.0	53.72	53.6	52.7	53.2	53.0	51.9	51.80	52.1	51.98
6	25.0	24.7	22.51	22.3	23.9	24.4	24.2	37.7	37.70	33.9	36.13*
7	106.5	106.2	106.39	106.2	104.4	105.9	105.7	57.7	-	56.3	58.40 weak
8	127.1	126.9	126.70	126.5	127.3	127.2	127.1	143.6	138.60*	146.3	138.15
9	118.2	118.0	118.51	118.3	117.2	118.0	117.8	124.7	124.56	123.6	123.47
10	119.6	119.4	119.65	119.5	118.4	119.4	119.2	126.4	126.23	125.7	125.61
11	121.6	121.5	121.78	121.6	120.5	121.5	121.3	129.0	128.81	128.3	128.19
12	111.0	110.9	110.97	110.8	110.9	111.0	110.8	121.6	120.2	121.1	119.93
13	136.7	137.0*	136.33	136.5*	136.9	136.7	137.4*	155.8	155.80 weak	155.7	156.10 weak
14	29.4	29.2	29.03	28.9	27.0	27.1	26.9	32.2	32.1	36.2	33.62*
15	29.6	29.4	30.74	30.6	27.7	27.4	27.2	34.2	34.2	32.6	32.50
16	55.6	50.3	53.58	53.4	43.9	44.0	43.8	70.2	67.80 weak	55.5	55.64
17	69.0	68.8	63.37	63.2	-	-	-	194.8	194.6	-	-
18	13.1	13.0	12.90	12.7	12.3	13.0	12.9	13.3	13.3	13.1	12.97
19	116.7	116.8	116.12	116.0	113.2	114.6	114.4	120.4	121.5	119.9	121.02
20	137.7	137.1*	136.74	136.9*	140.9	139.6	139.5*	138.5	143.30* weak	138.4	146.35
21	55.6	55.5	55.93	55.8	55.8	56.2	56.0	53.8	53.6	53.8	53.8
CH_3-O-<u>C</u>O	174.1	173.8	176.58	176.4	172.5	173.0	172.9	168.2	171.00 weak	171.8	171.8
<u>C</u>H_3-O-CO	51.5	50.6	52.35	52.2	49.8	50.8	50.9	52.8	52.6	51.7	51.7

* The assignments may be reversed.

Reference

1. Luca, V. D., Salim, V., Atsumi, S. M. & Yu, F. Mining the biodiversity of plants: a revolution in the making. *Science (New York, NY)* **336**, 1658–1661 (2012).

2. Guo, J., Gao, D., Lian, J. & Qu, Y. De novo biosynthesis of antiarrhythmic alkaloid ajmaline. *Nat. Commun.* **15**, 457 (2024).

3. Menzies, J. R. W., Paterson, S. J., Duwiejua, M. & Corbett, A. D. Opioid activity of alkaloids extracted from Picralima nitida (fam. Apocynaceae). *Eur. J. Pharmacol.* **350**, 101–108 (1998).

4. Kim, K. *et al.* Biosynthesis of kratom opioids. *N. Phytol.* **240**, 757–769 (2023).

5. Qu, Y. *et al.* Geissoschizine synthase controls flux in the formation of monoterpenoid indole alkaloids in a Catharanthus roseus mutant. *Planta* **25**, 1–10 (2017).

6. Qu, Y. *et al.* Solution of the multistep pathway for assembly of corynanthean, strychnos, iboga, and aspidosperma monoterpenoid indole alkaloids from 19 E-geissoschizine. *Proceedings Of The National Academy Of Sciences Of The United States Of America* **21**, 201719979–6 (2018).

7. Stavrinides, A. *et al.* Structural investigation of heteroyohimbine alkaloid synthesis reveals active site elements that control stereoselectivity. *Nature communications* **7**, 12116 (2016).

8. Stander, E. A. *et al.* The Rauvolfia tetraphylla genome suggests multiple distinct biosynthetic routes for yohimbane monoterpene indole alkaloids. *Commun. Biol.* **6**, 1197 (2023).

9. Scott, A. I. Biogenetic-type synthesis of the indole alkaloids. *Bioorganic chemistry* **3**, 398–429 (1974).

10. Dang, T.-T. T. *et al.* Sarpagan bridge enzyme has substrate-controlled cyclization and aromatization modes. *Nat Chem Biol* **14**, 760–763 (2018).

11. Wang, Z. *et al.* Deciphering and Reprogramming the Cyclization Regioselectivity in Bifurcation of Indole Alkaloids Biosynthesis. *Chem Sci* (2022) doi:10.1039/d2sc03612f.

12. Hong, B. *et al.* Biosynthesis of strychnine. *Nature* **607**, 617–622 (2022).

13. Eng, J. G. M. *et al.* A Catharanthus roseus Fe(II)/α-ketoglutarate-dependent dioxygenase catalyzes a redox-neutral reaction responsible for vindolinine biosynthesis. *Nat Commun* **13**, 3335 (2022).

14. Qu, Y., Safonova, O. & Luca, V. D. Completion of the canonical pathway for assembly of anticancer drugs vincristine/vinblastine in Catharanthus roseus. *The Plant journal : for cell and molecular biology* **97**, 257–266 (2018).

15. Caputi, L. *et al.* Missing enzymes in the biosynthesis of the anticancer drug vinblastine in Madagascar periwinkle. *Science (New York, NY)* **360**, 1235–1239 (2018).

16. Jarret, M. *et al.* Bioinspired Oxidative Cyclization of the Geissoschizine Skeleton for the Enantioselective Total Synthesis of Mavacuran Alkaloids. *Angewandte Chemie International Edition* 1–6 (2019) doi:10.1002/anie.201905227.

17. Benayad, S., Ahamada, K., Lewin, G., Evanno, L. & Poupon, E. Preakuammicine: A Long-Awaited Missing Link in the Biosynthesis of Monoterpene Indole Alkaloids. *European Journal of Organic Chemistry* **2016**, 1494–1499 (2016).

18. Qu, Y. *et al.* Completion of the seven-step pathway from tabersonine to the anticancer drug precursor vindoline and its assembly in yeast. *Proceedings of the National Academy of Sciences* **112**, 6224–6229 (2015).

19. Williams, D., Qu, Y., Simionescu, R. & Luca, V. D. The assembly of (+)-vincadifformine- and (−)-tabersonine-derived monoterpenoid indole alkaloids in Catharanthus roseusinvolves separate branch pathways. *The Plant journal : for cell and molecular biology* **99**, 626–636 (2019).

20. Kamileen, M. O. *et al.* Recycling Upstream Redox Enzymes Expands the Regioselectivity of Cycloaddition in Pseudo-Aspidosperma Alkaloid Biosynthesis. *J Am Chem Soc* (2022) doi:10.1021/jacs.2c08107.

21. Chatterjee, A., Banerji, A., Majumder, P. & Majumder, R. Alkaloids of Rhazya stricta Decaisne: Studies on Rhazinaline and Geissoschizine. *Bull. Chem. Soc. Jpn.* **49**, 2000–2004 (2006).

22. Yamauchi, T. *et al.* Alkaloids from the leaves of Alstonia scholaris in Taiwan, Thailand, Indonesia and the Philippines. *Phytochemistry* **29**, 3547–3552 (1990).

23. Levac, D., Cázares, P., Yu, F. & Luca, V. D. A Picrinine N-Methyltransferase Belongs to a New Family of γ-Tocopherol-Like Methyltransferases Found in Medicinal Plants That Make Biologically Active Monoterpenoid Indole Alkaloids. *Plant Physiol* **170**, 1935–1944 (2016).

24. Vrabec, R. *et al.* Monoterpene indole alkaloids from Vinca minor L. (Apocynaceae): Identification of new structural scaffold for treatment of Alzheimer's disease. *Phytochemistry* **194**, 113017 (2022).

25. Kohl, W., Witte, B. & Höfle, G. Alkaloide aus Catharanthus roseus-Zellkulturen, II [1] / Alkaloids from Catharanthus roseus Tissue Cultures, II [1]. *Zeitschrift Für Naturforschung B* **36**, 1153–1162 (1981).

26. Farzana, M. *et al.* Parallel evolution of methyltransferases leads to vobasine biosynthesis in Tabernaemontana elegans and Catharanthus roseus. *Front. Plant Sci.* **15**, 1451298 (2024).

27. Bartlett, M. F. *et al.* Rauwolfia Alkaloids. XXXVIII. 1 Stereospecific Degradations Leading to the Absolute Configurations and Structures of Ajmaline, Sarpagine and Corynantheidine 2. *J. Am. Chem. Soc.* **84**, 622–630 (1962).

28. Turpin, V., Poupon, E., Jullian, J. & Evanno, L. Biosynthetically Relevant Reactivity of Polyneuridine Aldehyde. *Eur. J. Org. Chem.* **2020**, 6989–6991 (2020).

29. Ahamada, K., Benayad, S., Poupon, E. & Evanno, L. Polyneuridine aldehyde: structure, stability overviews and a plausible origin of flavopereirine. *Tetrahedron Letters* **57**, 1718–1720 (2016).

30. Zhang, X. *et al.* Total Syntheses of Echitamine, Akuammiline, Rhazicine, and Pseudoakuammigine. *Angew. Chem. (Int. ed Engl.)* **58**, 6053–6058 (2019).

31. Kulagina, N., Méteignier, L.-V., Papon, N., O'Connor, S. E. & Courdavault, V. More than a Catharanthus plant: A multicellular and pluri-organelle alkaloid-producing factory. *Curr Opin Plant Biol* **67**, 102200 (2022).

32. Murata, J., Roepke, J., Gordon, H. & Luca, V. D. The leaf epidermome of Catharanthus roseus reveals its biochemical specialization. *The Plant cell* **20**, 524–542 (2008).

33. Mohammed, A. E. *et al.* Chemical Diversity and Bioactivities of Monoterpene Indole Alkaloids (MIAs) from Six Apocynaceae Genera. *Molecules* **26**, 488 (2021).

34. Il'yashenko, L. I., Malikov, V. M., Yagudaev, M. R. & Yunusov, S. Yu. Alkaloids of Vinca major. *Chem. Nat. Compd.* **13**, 324–327 (1977).

35. Bahadori, F. *et al.* Indole Alkaloids from Vinca major and V. minor Growing in Turkey. *Nat Prod Commun* **7**, 1934578X1200700610 (2012).

36. Boğa, M. *et al.* Two new indole alkaloids from Vinca herbacea L. *Phytochem. Lett.* **4**, 399–403 (2011).

37. Adizov, S. & Tashkhodjaev, B. Indole alkaloids from Vinca erecta type of sarpagine and ajmaline. *Eur. J. Chem.* **10**, 409–416 (2019).

38. Pfitzner, A. & Stöckigt, J. Polyneuridine aldehyde esterase: an unusually specific enzyme involved in the biosynthesis of sarpagine type alkaloids. *Journal of the Chemical Society, Chemical Communications* 459–460 (1983) doi:10.1039/c39830000459.

39. Dogru, E. *et al.* The gene encoding polyneuridine aldehyde esterase of monoterpenoid indole alkaloid biosynthesis in plants is an ortholog of theα/β hydrolase super family. *Eur J Biochem* **267**, 1397–1406 (2000).

40. Bayer, A., Ma, X. & Stöckigt, J. Acetyltransfer in natural product biosynthesis—functional cloning and molecular analysis of vinorine synthase. *Bioorganic & Medicinal Chemistry* **12**, 2787–2795 (2004).

41. Gerasimenko, I. *et al.* Purification and partial amino acid sequences of the enzyme vinorine synthase involved in a crucial step of ajmaline biosynthesis. *Bioorganic & Medicinal Chemistry* **12**, 2781–2786 (2004).

42. Schmidt, D. & Stöckigt, J. Enzymatic Formation of the Sarpagan-Bridge: A Key Step in the Biosynthesis of Sarpagine- and Ajmaline-Type Alkaloids. *Planta Medica* **61**, 254–258 (1995).

43. Pfitzner, A., Krausch, B. & Stöckigt, J. Characteristics of vellosimine reductase, a specific enzyme involved in the biosynthesis of the rauwolfia alkaloid sarpagine. *Tetrahedron* **40**, 1691–1699 (1984).

44. Corey, E. J. & Kim, C. U. New and highly effective method for the oxidation of primary and secondary alcohols to carbonyl compounds. *J. Am. Chem. Soc.* **94**, 7586–7587 (1972).

45. Méteignier, L.-V. *et al.* Harnessing the spatial and transcriptional regulation of monoterpenoid indole alkaloid metabolism in Alstonia scholaris leads to the identification of broad geissoschizine cyclase activities. *Plant Physiol. Biochem.* **219**, 109363 (2025).

46. Li, F. *et al.* Characterization of a vacuolar importer of secologanin in Catharanthus roseus. *Commun. Biol.* **7**, 939 (2024).

47. Li, C. *et al.* Single-cell multi-omics in the medicinal plant Catharanthus roseus. *Nat. Chem. Biol.* **19**, 1031–1041 (2023).

48. Sun, S. *et al.* Single-cell RNA sequencing provides a high-resolution roadmap for understanding the multicellular compartmentation of specialized metabolism. *Nat. Plants* **9**, 179–190 (2023).

49. Dang, T.-T. T., Franke, J., Tatsis, E. & O'Connor, S. E. Dual Catalytic Activity of a Cytochrome P450 Controls Bifurcation at a Metabolic Branch Point of Alkaloid Biosynthesis in Rauwolfia serpentina. *Angewandte Chemie International Edition* **56**, 9440–9444 (2017).

50. Lounasmaa, M. & Jokela, R. 1H- and 13C-Nmr Spectral Data of Five Sarpagine-type Alkaloids. *HETEROCYCLES* **43**, 1015 (1996).

51. Atta-ur-Rahman & Habib-ur-Rehman. Isolation and NMR Studies on Rhazimal and Strictamine. *Planta Med.* **52**, 230–231 (1986).